ACS APPLIED MATERIALS & INTERFACES

September 18, 2019
Volume 11
Number 37
pubs.acs.org/acsami

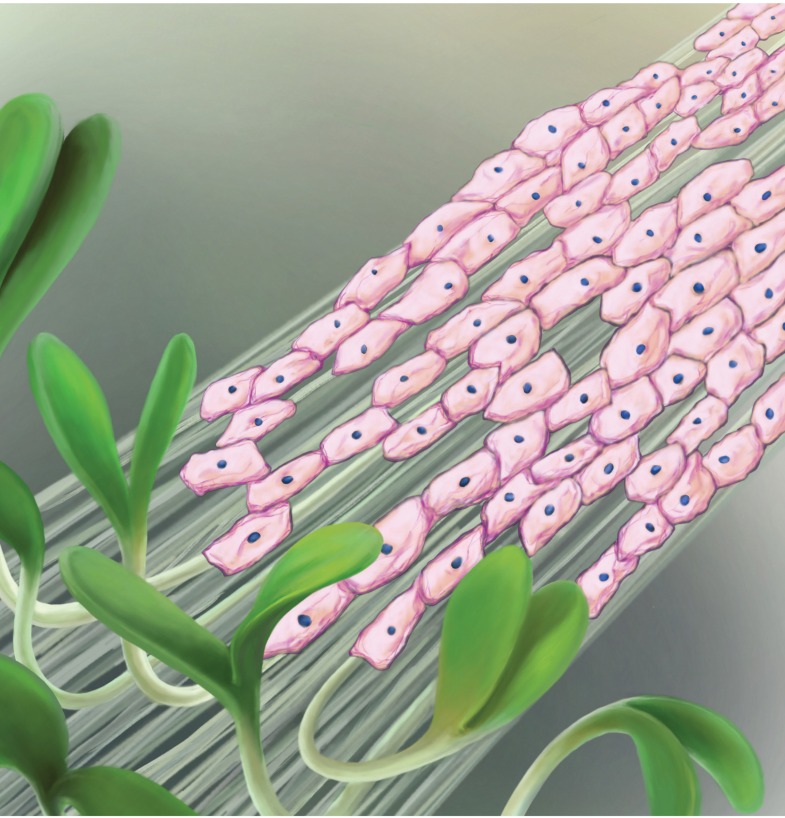

ACS Publications
Most Trusted. Most Cited. Most Read.

www.acs.org

ACS APPLIED MATERIALS & INTERFACES

Research Article

Cite This: ACS Appl. Mater. Interfaces XXXX, XXX, XXX−XXX

www.acsami.org

Alfalfa Nanofibers for Dermal Wound Healing

Seungkuk Ahn, Herdeline Ann M. Ardoña, Patrick H. Campbell, Grant M. Gonzalez, and Kevin Kit Parker*

Disease Biophysics Group, Wyss Institute for Biologically Inspired Engineering, John A. Paulson School of Engineering and Applied Sciences, Harvard University, Cambridge, Massachusetts 02138, United States

Supporting Information

ABSTRACT: Engineering bioscaffolds for improved cutaneous tissue regeneration remains a healthcare challenge because of the increasing number of patients suffering from acute and chronic wounds. To help address this problem, we propose to utilize alfalfa, an ancient medicinal plant that contains antibacterial/oxygenating chlorophylls and bioactive phytoestrogens, as a building block for regenerative wound dressings. Alfalfa carries genistein, which is a major phytoestrogen known to accelerate skin repair. The scaffolds presented herein were built from composite alfalfa and polycaprolactone (PCL) nanofibers with hydrophilic surface and mechanical stiffness that recapitulate the physiological microenvironments of skin. This composite scaffold was engineered to have aligned nanofibrous architecture to accelerate directional cell migration. As a result, alfalfa-based composite nanofibers were found to enhance the cellular proliferation of dermal fibroblasts and epidermal keratinocytes in vitro. Finally, these nanofibers exhibited reproducible regenerative functionality by promoting re-epithelialization and granulation tissue formation in both mouse and human skin, without requiring additional proteins, growth factors, or cells. Overall, these findings demonstrate the potential of alfalfa-based nanofibers as a regenerative platform toward accelerating cutaneous tissue repair.

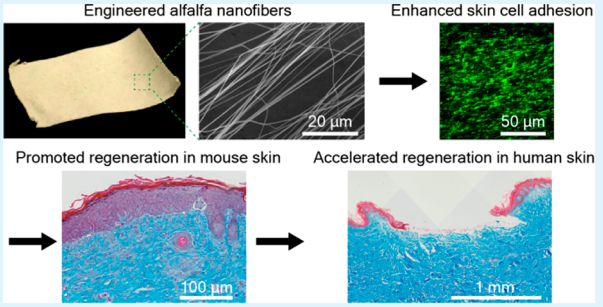

KEYWORDS: *alfalfa, herbal medicine, nanofiber, tissue engineering, wound healing*

Downloaded via HARVARD UNIV on August 14, 2019 at 21:34:18 (UTC).
See https://pubs.acs.org/sharingguidelines for options on how to legitimately share published articles.

INTRODUCTION

Cutaneous wounds from traumatic injury or chronic illness affect millions of patients worldwide.[1,2] Treatment of such wounds is challenging because skin regeneration is a spatiotemporally complex process that involves the migration of multiple types of cells toward the wound site.[3,4] This process occurs along with the intricate reorganization of nanofibrous extracellular matrix (ECM) networks.[3,4] Because of these convoluted repair processes, normal wound healing can only support a maladaptive regeneration of human skin. Scar formation is often the end result of the maladaptive healing, which is accompanied by a dense collagen matrix that obstructs the regeneration of hair follicles and cutaneous fat tissues.[5] Open wounds are also prone to infections because of microorganism invasion that can interfere with normal inflammatory response during the early stages of healing.[2] Collectively, the large population suffering from unhealed wounds and the complexity of the healing process substantiate the pressing need for developing wound dressings that (1) absorb wound exudates (e.g., blood, plasma); (2) protect wounds from infection; (3) prevent further mechanical damage; and most importantly, (4) can accelerate skin regeneration.[6−10]

Currently, a variety of commercial wound dressings have been developed to retain a moist environment (e.g., hydrocolloid dressings) and to further accelerate skin regeneration using bioactive components (e.g., dermal template).[11] The utility of nanofiber scaffolds has recently received considerable attention, as they recapitulate the fibrous architecture of native tissue microenvironments that is crucial for homeostasis and wound repair in cutaneous ECM.[12−14] For instance, nanofiber scaffolds built from fibronectin, one of the main ECM proteins in skin, promoted wound closure and skin appendage regeneration.[15] Plant-derived components are also currently being explored as a novel source for nanofiber scaffold materials to improve cost efficiency, prevent immunogen transfer and advance compositional definition.[16−20] In particular, soy protein nanofiber scaffolds have been previously reported to accelerate wound closure and reduce scar formation.[20] However, the limited range of plant types and processing techniques, as well as the lack of a systematic understanding of their regenerative mechanisms, constrain the utility of plant-based bioscaffolds.

Alfalfa (*Medicago sativa*), an ancient herbal medicine that is considered as "father of all foods," has been used in oral and topical treatments for healing cutaneous wounds.[21−23] Mechanistic and clinical studies reported that the medicinal effects of alfalfa can be attributed to bioactive components, such as phytoestrogens and chlorophylls.[21] Phytoestrogens

Received: May 8, 2019
Accepted: August 1, 2019
Published: August 1, 2019

© XXXX American Chemical Society

DOI: 10.1021/acsami.9b07626
ACS Appl. Mater. Interfaces XXXX, XXX, XXX−XXX

such as genistein are structural analogs of estrogen,[23,24] which bind to estrogen receptor (ER)-β to activate the ER-β pathways for accelerating wound closure and tissue remodeling.[24−28] In addition, chlorophylls in alfalfa can facilitate antibacterial activity and oxygenation at wound sites.[21,29,30] Although the therapeutic potential of alfalfa and its associated mechanisms have been established,[21,23] alfalfa has not yet been explored as a component for developing regenerative wound dressings.

In this study, we hypothesize that alfalfa-based nanofibers can provide cutaneous ECM-mimetic nanostructures and bioactive molecules to enhance the rate of skin regeneration. These bioactive components were stabilized within the scaffolds by the generation of polycaprolactone (PCL) and alfalfa composite fibers using a high-throughput nanofiber manufacturing system called pull spinning.[31] The physical and chemical properties of these nanofibers were engineered to recapitulate native skin microenvironments while carrying chlorophylls and genistein. The PCL/alfalfa nanofiber scaffolds accelerated the growth of dermal fibroblasts and epidermal keratinocytes in vitro, promoted tissue repair in vivo in mice and ex vivo in human wound models.

MATERIALS AND METHODS

Materials. PCL (M_n 80,000; Sigma-Aldrich, USA), alfalfa (powdered alfalfa leaf; Frontier Natural Products Co-op, USA), and 1,1,1,3,3,3-hexafluoro-2-propanol (HFIP; Oakwood Chemical, USA) were used in this study.

Fiber Spinning. Pull spinning was used to produce nanofibers as described previously.[31] In brief, different concentrations of alfalfa were dissolved in HFIP with 6 wt/v% PCL. The solution was stirred overnight. The prepared solution was pumped at 0.3 mL/min and contacted with the rotating bristle at 25 000 rpm to form nanofibers. The spun nanofibers were dried in a chemical hood overnight to remove excess HFIP before further characterization. For in vitro cell culture studies, the nanofibers were directly spun on glass coverslips.

Scanning Electron Microscopy (SEM). The spun nanofibers were mounted on SEM stubs and sputter-coated with Pt/Pd (5 nm thickness, Denton Vacuum, USA) before imaging. The samples were imaged using field emission scanning electron microscopy (FESEM Supra 55VP, Zeiss, USA).

Fiber Diameter, Alignment, and Porosity Analysis. SEM images of nanofibers were used to quantitatively determine the fiber diameter, alignment, and porosity. The analysis was performed by utilizing ImageJ software (NIH) with the DiameterJ and Orientation J plug-ins.[32,33] The % porosity was calculated by dividing the pore area (the total number of black pixels in a binary image) by the total area (the total number of pixels in a binary image). For the fiber alignment analysis, the Orientation J plug-in generated the distribution of the alignments for all pixels according to the structure tensor. Afterward, Gaussian fitting was applied to the raw data to show the anisotropic distribution of fiber alignment by using OriginPro 8.6 software (Origin Lab Corporation).

Fourier Transform Infrared Spectroscopy. The IR spectra of nanofibers were recorded using an attenuated total reflectance-Fourier transform infrared spectrometer (ATR-FTIR, Lumos, Bruker, USA). The raw spectra were normalized from 0 to 1. OriginPro 8.6 software was used to plot the normalized spectra.

UV−Vis Absorption Spectroscopy. The absorption spectra of nanofiber membranes were recorded using a Cary 60 UV−vis spectrometer (Agilent, USA). The absorption spectra were collected from 400 to 800 nm.

Hyperspectral Imaging. PCL and PCL/alfalfa fibers cast on silicon wafers were imaged in reflectance mode using a darkfield hyperspectral microscope (Cytoviva) integrated with a confocal Raman microscope (Horiba XploRA PLUS). Hyperspectral maps were processed using ENVI data analysis software (ENVI Classic 5.4) to reconstruct the spectral information for multiple regions of interest per fiber. The corresponding darkfield images were obtained using a 50× objective under a halogen lamp (International Light Technologies Part L1090, USA).

Contact Angle Measurement. To measure contact angles, the cast films were prepared by pouring and drying the polymer solution in a Petri dish overnight at room temperature. Ten microliters of water were dropped on the surface of the samples, after which droplet formation was imaged. ImageJ software with the Drop Shape Analysis plug-in was used to calculate the contact angle.[34]

Mechanical Property Testing. The single fiber standard ASTM D3822M-14 was adapted to determine the modulus of fiber sheets. A frame cut from a 130 μm thick polycarbonate sheet was employed to ensure that there was no fiber slippage at the fiber clamp interface. The frame had a gauge length of 2.5 mm to match the length of the fibrous scaffolds tested for in vitro cell culture. Fiber samples were cut to 10 mm length and secured to the frame using a primer (Loctite 770, USA), followed by the application of an adhesive (Loctite 401) to ensure that there was no slippage between the frame and the fiber. After preparation, a frame loaded with a sample was placed into the pneumatic grips of an Instron model 5566 equipped with a 10 N Load Cell. After loading, the frame was cut to allow for extension of the fiber sheets. The sample was then strained at a rate of 240% per min until sample breaking.

Liquid Chromatography−Mass Spectrometry. The amount of genistein in alfalfa powder and nanofibers was measured by using liquid chromatography−mass spectrometry (LC-MS, Agilent 1290/6140, USA) with selected ion monitoring (SIM) mode. Samples were prepared in dimethyl sulfoxide (DMSO, HPLC grade, Sigma-Aldrich, USA). A gradient of H_2O and acetonitrile (ACN) with a flow rate of 0.25 mL/min was selected as the mobile phase for the C18 LC column (ZORBAX RRHD C18, USA). The gradient was as follows. A ratio of 95% H_2O and 5% ACN was maintained for the first 2 min. Then, the ratio increased to 100% B over 10 min. Then, 100% B was retained for 2 min and decreased to 95% A and 5% B over 1 min. After chromatographic separation, electrospray ionization (ESI) mode was applied to ionize molecules and thus detect ions based on their molecular weights. For genistein detection, negative ESI-MS scans at m/z 269 were performed with SIM to increase sensitivity to the genistein-specific peak at m/z 269. For profiling genistein release, nanofibers were submerged in phosphate-buffered saline (PBS, Invitrogen, USA) solution at 37 °C. PBS solution and the nanofibers were collected after 12, 24, and 48 h incubation. Samples were dried and then dissolved in DMSO for LC-MS measurement as described above.

Human Dermal Fibroblast and Keratinocyte Culture. Green fluorescent protein (GFP)-expressing HNDFs (Angio-Proteomie, USA) and adult human epidermal keratinocytes (HEKa cells, ATCC, USA) were cultured on nanofibers. HNDFs were subcultured to passage 7 in Dulbecco's modified Eagle's medium (DMEM, Thermo Fisher Scientific, USA) with 5% fetal bovine serum (FBS) and 1% antibiotics (penicillin/streptomycin, Thermo Fisher Scientific). HEKa cells were subcultured to passage 5 in dermal cell basal medium (ATCC, USA) with a keratinocyte growth kit (ATCC, USA). Both HNDFs and HEKa cells were passaged by using 0.25% trypsin-ethylenediaminetetraacetic acid solution (trypsin/EDTA, Lonza, USA). For HNDF and HEKa cell culture, we seeded 100 000 cells per sample in 6-well plates. The cell culture media were replaced every 2 days.

HEKa cells were cultured for 7 days and then fixed with 4% paraformaldehyde (PFA), followed by permeabilization with 0.05% Triton X-100 for 10 min. The fixed samples were then incubated with 5% bovine serum albumin (BSA, Sigma-Aldrich, USA) for 2 h at room temperature to block nonspecific binding. After blocking, the samples were incubated with a primary antibody (anticytokeratin 14 or K14, Abcam, USA) in 0.5% BSA for 1 h at 37 °C, followed by an Alexa Fluor 488-conjugated mouse IgG (H+L) secondary antibody (Invitrogen, USA) and 4′,6-diamidino-2-phenylindole dihydrochloride (DAPI, Invitrogen, USA) for 1 h at 37 °C. The samples were

DOI: 10.1021/acsami.9b07626
ACS Appl. Mater. Interfaces XXXX, XXX, XXX−XXX

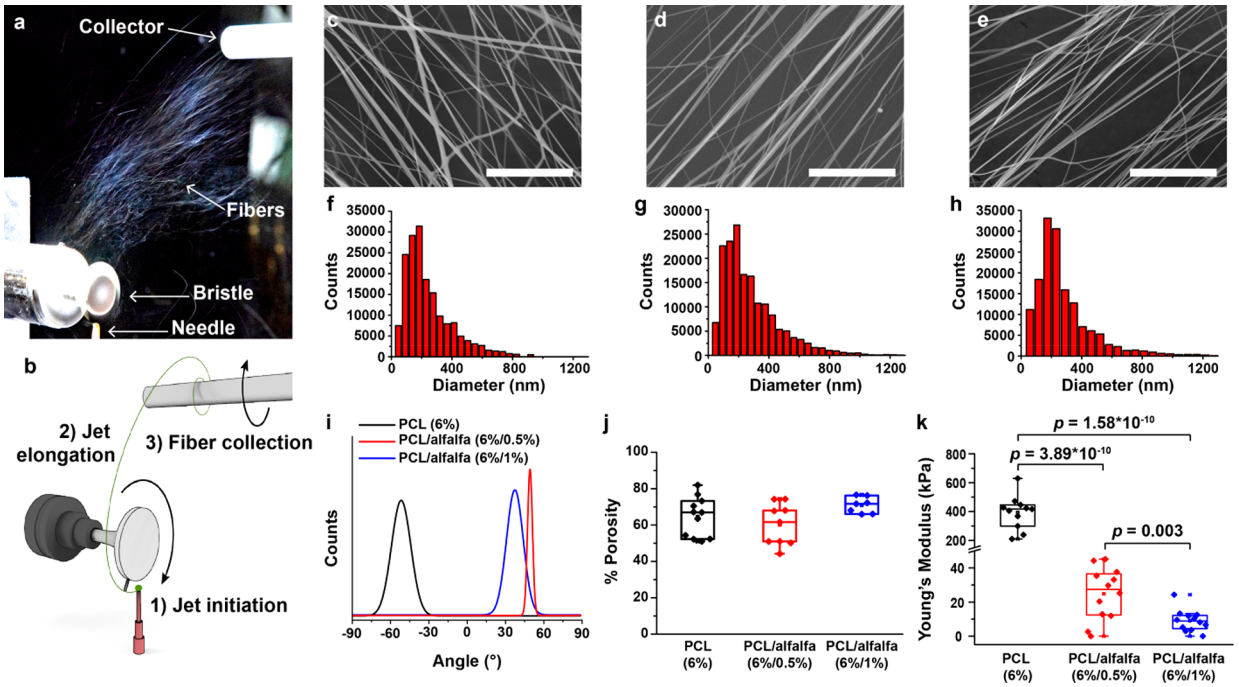

Figure 1. Nanofiber fabrication. (a, b) Pull spinning system: (a) representative image and (b) schematic diagram of the setup; (c–e) SEM images, (f–h) fiber diameter analysis, (i) alignment analysis, and (j) porosity analysis of PCL (6 wt/v%), PCL/alfalfa (6 wt/v%/0.5 wt/v%), and PCL/alfalfa (6 wt/v%/1 wt/v%) nanofibers. The scale bars of the SEM images are 20 μm. For statistical analysis in f–j, $n = 4$ and field of view (FOV) ≥ 4. The edges of the box plots in (j) were defined as the 25th and 75th percentiles. The middle bar is the median, and the whiskers are the 5th and 95th percentiles. For the fiber alignment analysis, Gaussian fits were applied to the raw data to show the distribution of fiber directionality. (k) Young's modulus of nanofiber scaffolds. For statistical analysis, $n = 12$ and $^*p < 0.05$. The edges of the box plots were defined as the 25th and 75th percentiles. The middle bar is the median, and the whiskers are the 5th and 95th percentiles.

mounted on glass slides and imaged immediately using a spinning disc confocal microscope (Olympus ix83, USA).

Cytotoxicity Measurement. The cytotoxicity of nanofibers was investigated using a commercial lactic acid dehydrogenase (LDH) assay (Promega, USA).[20,35] The cell culture media were collected at day 7 of cell culture. The collected media were incubated with the reagent for 30 min at room temperature. Then, stop solution was added to the samples, and the absorbance of the solutions was measured at 490 nm using a microplate reader (BioTek, USA).

Cell Coverage Analysis. GFP-expressing HNDFs and HEKa cells on nanofibers at day 0 (6 h after cell seeding) and day 7 of cell culture were imaged using confocal microscopy. The cell coverage was analyzed using ImageJ to calculate the area percentage of the GFP-positive area for HNDFs and the K14-positive area for HEKa cells from the confocal images. The cell coverage was then normalized to the average cell coverage on PCL scaffolds at day 0.

Mouse Excisional Wound Splinting Model. All animal experiments for the wound healing study were approved by the IACUC. As previously reported,[36] we utilized the mouse splinting model to limit wound contraction in the mouse skin in an effort to investigate human-like wound healing. Briefly, C57BL/6 male mice (8 weeks old, Charles River Laboratories, USA) were anesthetized using isoflurane during all procedures. The hair on the dorsal side of the mice was shaved using an electric razor. After shaving, betadine (Santa Cruz Biotechnology, USA) and ethanol (70% vol/vol) were used to clean the skin. Full-thickness wounds (2 wounds per mouse) were made by utilizing a 6 mm diameter sterile biopsy punch (Integra Miltex, USA). The splinting rings were attached to the skin near the wound sites with an adhesive (Krazy glue, USA) and sutures (Ethicon, USA). We applied nanofiber scaffolds, 3 M Tegaderm hydrocolloid dressing (3M, USA), and Hollister Endoform dermal template collagen dressing (Hollister Incorporated, USA) to the wounds and then covered the wounds with Tegaderm waterproof transparent dressing (Nexcare, USA) patches. For control samples, the wounds received no treatment but were covered with Tegaderm patches.

For quantitative wound healing analysis, epithelial gaps and granulation tissue formation were analyzed from Masson's trichrome images following the established methods.[36] Wound closure was monitored on days 0 and 14 after the surgery. Tissues were harvested on day 14 postsurgery. The harvested tissues were fixed with 4% PFA, embedded in paraffin, sectioned, deparaffinized, and stained with Masson's trichrome. Masson's trichrome-stained samples were imaged by a slide scanner (Olympus VS120, USA). In an effort to quantitatively evaluate the efficacy of engineered scaffolds, we utilized a skin tissue architecture quality (STAQ) index, as reported in a recent publication.[15] This computer code was written by using Python software (v 2.5, Python). In brief, the STAQ index uses a modified version of the Hellinger distance metric to measure the overlap in values between healthy and healed skin.[15]

For immunochemistry, the sections were deparaffinized and incubated with 5% BSA for 2 h. Then, the sections were incubated with primary antibody (anti K14) in 1% BSA overnight at 4 °C. Next day, the samples were washed with PBS 3 times and incubated with secondary antibodies (Alexa Fluor 488-conjugated mouse IgG (H+L) secondary antibody and DAPI) for 1h. After the incubation, the samples were washed with PBS 3 times and then imaged using a spinning disc confocal microscope (Olympus ix83, USA).

Tissues harvested on day 0 were used to assess the architecture of normal skin tissues. The collected tissues were fixed with 4% PFA, embedded in paraffin, sectioned, deparaffinized, and dried for SEM imaging. The samples were then mounted on SEM stubs, sputter-coated with Pt/Pd (5 nm thickness), and then imaged by using FESEM. The fiber diameter was analyzed by using ImageJ software with the DiameterJ plug-in.[32]

Ex Vivo Human Skin Wound Model. A human skin model (NativeSkin, Genoskin) with 2 mm wounds was purchased and cultured for up to 7 days with dedicated culture medium according to the manufacturer's instructions.[37] The donor was a 45-year-old

DOI: 10.1021/acsami.9b07626
ACS Appl. Mater. Interfaces XXXX, XXX, XXX–XXX

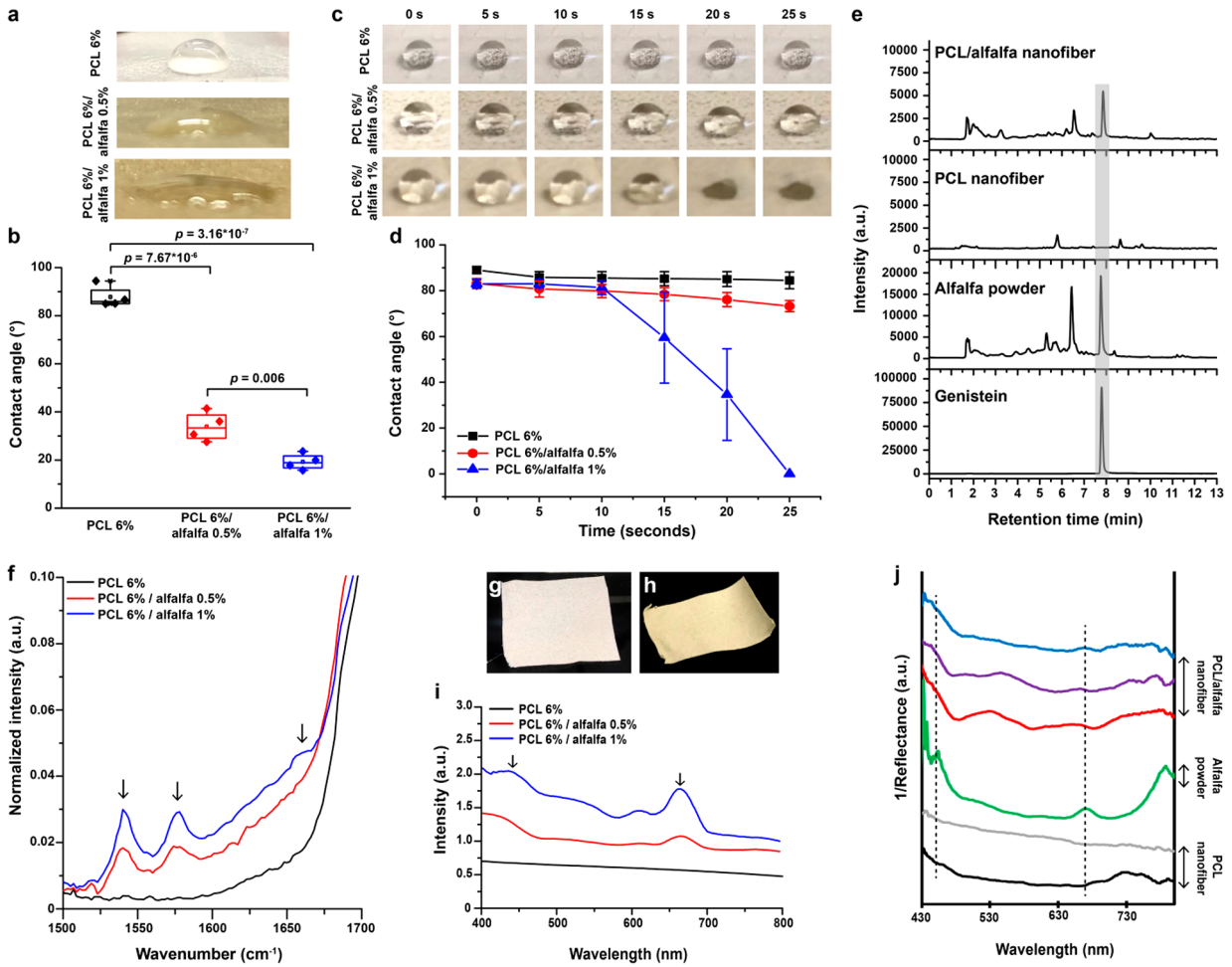

Figure 2. Chemical properties of alfalfa scaffolds. (a–d) Contact angle measurements of (a, b) cast films and (c, d) nanofibers. For statistics, (b) $n = 4$ and (d) $n = 3$. The edges of the box plots in b were defined as the 25th and 75th percentiles. The middle bar is the median, and the whiskers are the 5th and 95th percentiles. Error bars in d represent standard error of mean. (e) Phytoestrogen (genistein) analysis by LC-MS. The gray box indicates the genistein-specific peak ($m/z = 269$). (f) FT-IR spectra of nanofibers. Black arrows indicate amide peaks. (g–i) Representative images of (g) PCL (6 wt/v%) and (h) PCL/alfalfa (6 wt/v%/1 wt/v%) nanofibers with (i) corresponding UV–vis absorption spectra. Black arrows indicate absorbance peaks specific to alfalfa (λ_{max}= 435, 663 nm). (j) Hyperspectral imaging spectra of alfalfa film, PCL nanofibers, and PCL/alfalfa nanofibers.

Caucasian female. Tissues were collected from the donor's abdomen, wounded with a 2 mm biopsy punch, and embedded in the nourishing solid matrix at day 0.[37] Immediately after receiving the samples on day 1, we applied nanofiber scaffolds, 3 M Tegaderm hydrocolloid dressing, or Hollister Endoform dermal template collagen dressing to the wounds. After 7 days of culture (maximum culture time), tissues were collected, fixed with 4% PFA, embedded in paraffin, sectioned, deparaffinized, and stained with Masson's trichrome. The stained tissues were imaged by a slide scanner (Olympus VS120, USA). The epithelial gap was analyzed from Masson's trichrome images following the established method.[36]

Statistical Analysis. All data are presented as the mean ± standard error (SEM) and box plots with all data points overlapping. The edges of the box plots were defined as the 25th and 75th percentiles. The middle bar is the median, and the whiskers are the fifth and 95th percentiles. Statistical comparisons using one-way analysis of variance (ANOVA) with post hoc Tukey's test and Grubb's test (to evaluate outliers) at the 0.05 significance level were calculated using OriginPro 8.6 software. *p values less than 0.05 were considered statistically significant.

RESULTS

Nanofiber Fabrication and Mechanical Property Characterization. To mimic the native cutaneous microenvironment,[3] we fabricated nanofibers using a pull spinning system under high centrifugal forces (Figure 1a, b).[15,31,38−45] Alfalfa was cospun with PCL, which is a common carrier polymer in nanofiber production due to its fiber-forming capability, biocompatibility and biostability.[46] Specifically, 6 wt/v% PCL was added as a carrier polymer because this formulation was previously used to create nanofibers without bead formation.[31] Hexafluoro-2-propanol (HFIP) was applied here as the solvent for the composite polymer dope since it is volatile and can dissolve both PCL and the biomolecular contents of alfalfa. The concentration of alfalfa (0, 0.5, and 1 wt/v%) was varied with a fixed ratio (6 wt/v%) of PCL in HFIP (Table S1). Without the cospinning polymer, alfalfa alone cannot form fibers (Figure S1a) due to its low chain entanglement. When cospun with PCL, the spinning conditions generated continuous nanofibers (Figure 1c–e) with diameters of 345.3 ± 52.5 nm for PCL 6 wt/v%, 394.3 ± 70.7 nm for PCL 6 wt/v%/alfalfa 0.5 wt/v%, and 408.6 ± 56.1 nm for PCL 6 wt/v%/alfalfa 1 wt/v% (Figure 1f–h). When the doping concentration was 1.5 wt/v% or higher, the spun nanofibers exhibited extreme bead formation (Figure S1b,c). The fiber diameter increased when the ratio of alfalfa increased

DOI: 10.1021/acsami.9b07626
ACS Appl. Mater. Interfaces XXXX, XXX, XXX−XXX

in the polymer dope. Previously, we described that fiber morphology (e.g., preventing bead formation) and diameter can also be controlled by adjusting the tip-to-collector distance and bristle rotation speed.[31] However, polymer concentration imparts significantly greater influence to fiber morphology and diameter as compared to collector distance and bristle rotation speed.[31] Similar to the engineered nanofibers, the normal skin also showed nanofibrous structure with a fiber diameter of 279.5 ± 112.8 nm in the dermal collagenous fiber area (Figure S2), which is consistent with previous studies.[47−49] Along with the topographical aspect of the nanofibers, fiber alignment was also incorporated into our design criteria to provide directional cues for accelerating cellular migration during wound healing.[48,50] The spun nanofibers were verified to have a unidirectional distribution of fiber orientation (Figure 1i). Furthermore, the porosity of these nanofiber scaffolds did not change across the different alfalfa doping concentrations (Figure 1j). These data suggest that our scaffolds successfully mimic the nanofibrous architecture of skin, which is important for providing structural support to the cells.

In addition, scaffold stiffness plays a crucial role in wound healing.[51] Cells prefer to adhere to and proliferate on substrates that have a stiffness similar to that of the native tissues from which the cells originate.[52] Accordingly, mechanical matching of scaffolds to the tissue is an important factor for tissue engineering applications because the stiffness of human tissues varies according to structure and function—ranging from a few hundred Pa (brain) to a few GPa (bone).[53] In particular, the stiffness of the human dermis is within a range of a few tens of kPa depending on the region of the body and the method selected for measurement.[54−56] To determine whether these native dermal features were reflected in our engineered nanofibers, mechanical uniaxial testing was performed (Figure 1k). The Young's modulus values of the PCL/alfalfa scaffolds were 24.9 ± 4.4 kPa (with 0.5 wt/v% alfalfa) and 9.0 ± 1.8 kPa (with 1 wt/v% alfalfa), whereas that of the PCL scaffolds was 394.3 ± 35.0 kPa. The Young's modulus of the nanofiber scaffolds significantly decreased as the concentration of alfalfa doping increased. The mechanical properties of these alfalfa-based nanofibrous scaffolds, which are within the range of the human dermis.[57]

Chemical Properties of Nanofiber Scaffolds. To attract cells into the wound and to potentiate the removal of cellular debris, it is important that dressings provide a moist environment with hydrophilic surfaces.[58−60] Superhydrophilic surfaces can be advantageous for wound healing applications since they promote cell adhesion, proliferation, infiltration, and ultimately new tissue formation.[61] Because the hydrophilicity of a material affects its efficacy as a bioscaffold, we measured the wettability of our alfalfa-based scaffolds. The contact angle (θ) was used to classify the surface wettability as follows: superhydrophilicity ($\theta < 25°$), high hydrophilicity ($25° < \theta < 90°$), low hydrophilicity ($90° < \theta < 150°$), and superhydrophobicity ($\theta > 150°$).[62] These values were measured for both cast films and nanofiber scaffolds by calculating the angles between a water droplet and the surface of the composite materials. For cast films, measuring contact angles is a traditional way to investigate static wettability (Figure 2a,b). The contact angle on the PCL cast film was measured as 86.4° ± 2.3, which is close to low hydrophilicity because of the hydrophobic nature of the PCL. With the addition of alfalfa, the cast film (6 wt/v% PCL/1 wt/v% alfalfa) became more hydrophilic and exhibited a superhydrophilic surface (θ = 17.9 ± 1.7°).

For spun nanofiber scaffolds, the measured contact angles do not represent conventional static wettability because of the porous nature of the scaffold (Figure 2c, d). Rather, these measurements explain the degree of spreading and absorption of the droplet on the scaffolds.[62] The initial contact angles under all conditions were similar regardless of the chemical compositions. However, within the same time frame (25 s), water droplets on PCL/alfalfa (6 wt/v%/1 wt/v%) nanofiber scaffolds completely spread and were absorbed, resulting in a superhydrophilic contact angle (~0°). On the other hand, PCL-only and PCL/alfalfa (6 wt/v%/0.5 wt/v%) nanofiber scaffolds retained water droplets on their surfaces at 25 s, with high contact angles ($\theta > 70°$). Because nanofiber scaffolds are absorptive materials and have higher roughness than cast films, the contact angles of nanofiber scaffolds at later time points are lower than those of cast films. Moreover, the hydrophilic components of alfalfa (such as proteins and phytoestrogens) increase wettability by facilitating the interaction between the surface of the material and the polar water droplet. Therefore, in subsequent experiments, the superhydrophilic PCL/alfalfa (6 wt/v%/1 wt/v%) composite nanofibers were selected as the material of choice for the bioscaffolds used to explore the effect of alfalfa in nanofibers on wound healing. On the other hand, PCL nanofibers served as the control group for these experiments to investigate the effects of alfalfa within the scaffolds.

To test if the biomolecular components of alfalfa remained stable during the fiber spinning process, a series of chemical characterizations of the composite nanofibers were conducted. First, LC-MS analysis was carried out to verify the presence of genistein (Figure 2e), which is one of the major phytoestrogens in alfalfa. Accordingly, a signal at m/z = 269 was detected using selected ion monitoring (SIM) mode to quantify the amount of genistein. The elution time for a standard solution of genistein was observed at 7.8 min. The same peak at 7.8 min was also found in alfalfa powder and PCL/alfalfa nanofibers but not in PCL nanofibers, which indicates the genistein content in PCL/alfalfa nanofibers. The amount of genistein in PCL/alfalfa nanofibers was measured, which was 2.48 ± 1.02 mg/L (analyzed from 5 samples). On the other hand, the amount of genistein in the alfalfa only dope was 3.24 ± 0.23 mg/L (analyzed from 3 samples). These data indicate that the pull spinning system allowed for 76.5% of genistein from the original alfalfa only dope to be incorporated within the alfalfa-based nanofibers. We also measured the release kinetics of genistein from PCL/alfalfa nanofibers (Figure S3). Under physiologically relevant conditions (submerged in PBS solution at 37 °C), the nanofibers showed a burst release of genistein within 2 days because of the fast dissolution of alfalfa components, mirroring the characteristic release kinetics of most nanofibers that are noncovalently loaded with small molecules.[20,63] Consequently, genistein, which accelerates wound healing, may be delivered by using the PCL/alfalfa nanofibers fabricated herein. Although purified genistein or chlorophylls have been previously integrated into bioscaffolds,[64−67] additional purification procedures to obtain these molecules from plants require multiple steps and thereby may increase manufacturing cost and time.[30,68] Accordingly, using alfalfa as a building block offers a comprehensive and scalable approach to incorporate multiple bioactive compounds in wound dressings.

DOI: 10.1021/acsami.9b07626
ACS Appl. Mater. Interfaces XXXX, XXX, XXX−XXX

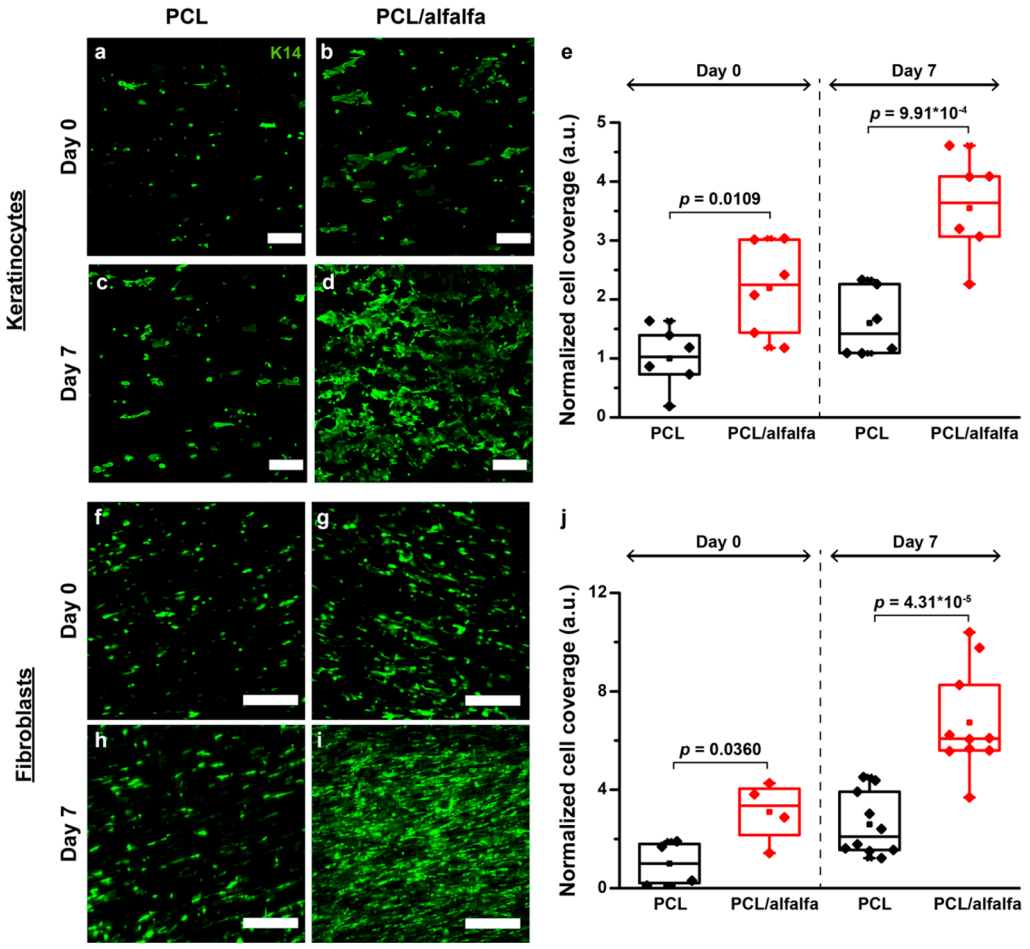

Figure 3. In vitro epidermal and dermal cell culture. Representative immunofluorescence images of (a–d) HEKa cells cultured on PCL and PCL/alfalfa nanofiber scaffolds at day 0 (6 h after seeding) and day 7 with (e) cell coverage analysis. The scale bars of a–d HEKa cells are 200 μm. (f–j) Representative immunofluorescence images of (f–i) GFP-expressing HNDFs cultured on PCL and PCL/alfalfa nanofiber scaffolds at day 0 (6 h after seeding) and day 7 with (j) cell coverage analysis. The scale bars of f–i HNDFs are 50 μm. $n = 6$ for HEKa cells and $n = 4$ for HNDFs at day 0 and $n = 10$ for HNDFs at day 7. *$p < 0.05$. The edges of the box plots in e and j were defined as the 25th and 75th percentiles. The middle bar is the median, and the whiskers are the 5th and 95th percentiles.

We then examined the FT-IR spectra of the nanofibers (Figure 2f) to assess the protein content of the alfalfa scaffolds. The FT-IR spectra showed a major peak at 1723 cm^{-1}, which is indicative of carbonyl stretching (C═O) of PCL.[50] All spectra were normalized to the PCL peak (1732 cm^{-1}) to observe relative changes in IR peaks. To verify the presence of alfalfa in the nanofibers, we measured amide peaks, because PCL has no peak in the amide I and II regions (1500–1700 cm^{-1}). The amide peaks at 1540, 1578, and 1660 cm^{-1} increased with higher alfalfa concentrations.

The optical properties of PCL/alfalfa composite nanofibers also showed a distinctive green color due to the high chlorophyll content in the native state of alfalfa, whereas PCL-only nanofibers did not (Figure 2g,h). The UV–vis absorption spectra of PCL/alfalfa nanofibers showed peaks at ~450 and ~650 nm,[69] which are indicative of chlorophyll content, whereas no peaks were detected for PCL nanofibers (Figure 2i). Nanofibers with higher alfalfa concentrations resulted in stronger peak intensities at 435 and 663 nm. This finding was further confirmed using hyperspectral imaging (Figure 2j), whereby the average absorbance map was collected from multiple regions of samples. In line with the UV–vis absorption data, the alfalfa cast film showed distinctive peaks (at ~435 and 663 nm) due to the chlorophyll content of alfalfa, which are consistent with the peaks detected in the different regions of the PCL/alfalfa nanofibers and are not present in the spectra for the PCL nanofibers. Altogether, these results indicate that the bioactive components of alfalfa, particularly genistein and chlorophylls, were successfully integrated within the PCL/alfalfa composite scaffolds even after the fiber spinning process.

In Vitro Skin Cell Culture. In previous sections, the nanofibrous and superhydrophilic nature of PCL/alfalfa scaffolds were characterized, along with their bioactive contents, which are crucial for accelerating the processes involved in wound healing. We then asked whether PCL/alfalfa nanofiber scaffolds can support skin cell viability, adhesion, and proliferation. PCL/alfalfa nanofiber scaffolds were used as substrates to culture two types of skin cells: adult human epidermal keratinocytes (HEKa cells) and human neonatal dermal fibroblasts (HNDFs) (Figure 3). PCL nanofibers served as a control group to determine whether the presence of alfalfa in the nanofibers can enhance skin cell growth. First, the biocompatibility of PCL/alfalfa nanofibers was investigated by utilizing a traditional lactate dehydrogenase (LDH) assay to measure the LDH release from necrotic cells.[35] After 7 days of culture, both HEKa cells and HNDFs on PCL and PCL/alfalfa nanofibers released similar amounts

DOI: 10.1021/acsami.9b07626
ACS Appl. Mater. Interfaces XXXX, XXX, XXX–XXX

of LDH without a statistically significant difference, demonstrating the biocompatibility of PCL/alfalfa nanofibers (Figure S4a, b). Additionally, both HEKa cells and HNDFs showed anisotropic growth along the fiber axis (Figure 3). PCL/alfalfa nanofibers showed higher HEKa cell adhesion and growth at day 0 (6 h after seeding) compared to PCL nanofibers (Figure 3a, b). After 7 days of culture, HEKa cell coverage remained significantly higher on PCL/alfalfa nanofibers than on PCL nanofibers (Figure 3c–e). Similarly, HNDFs coverage on PCL/alfalfa nanofibers was also higher than on PCL nanofibers at both day 0 and 7 (Figure 3f–j). These data indicate that the increased hydrophilicity due to the existence of bioactive components in alfalfa-containing fibers contributed to enhanced cell growth on the composite bioscaffolds. Taken together, these in vitro cell culture experiments suggest that PCL/alfalfa nanofiber scaffolds can promote cell growth and sustain biocompatibility for epidermal keratinocytes and dermal fibroblasts to accelerate skin tissue regeneration. These findings demonstrate the potential applicability of alfalfa nanofibers toward facilitating skin regeneration.

In Vivo Regeneration of Mouse Skin. In an effort to test the regenerative potency of PCL/alfalfa scaffolds in vivo, an excisional mouse splinting wound model was applied to study how our scaffolds affect tissue regeneration (Figure 4a). This

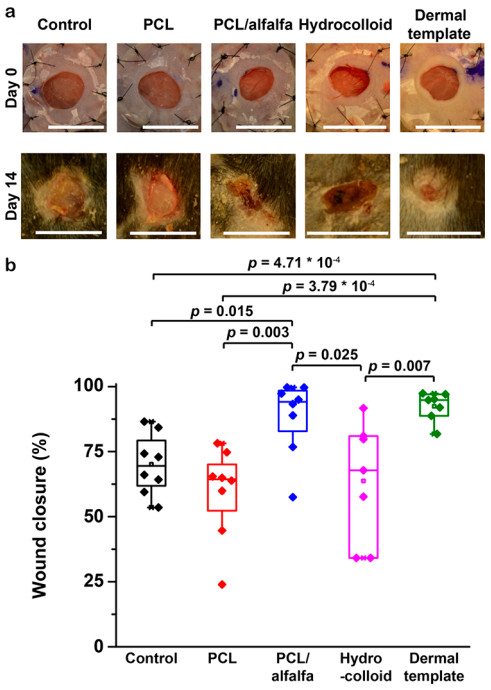

Figure 4. In vivo mouse wound closure. (a) Representative images of wounds at days 0 and 14 postsurgery with (b) wound closure analysis at day 14 postsurgery. The scale bars in a are 10 mm for day 0 and 5 mm for day 14. *$p < 0.05$ and $n = 6$. The edges of the box plots in b were defined as the 25th and 75th percentiles. The middle bar is the median, and the whiskers are the 5th and 95th percentiles.

model limits wound contraction in mice, which therefore allows for a closer representation of human wound healing as compared to a nonsplinting mouse model.[36,70,71] The control wounds received no treatment but were covered with Tegaderm waterproof transparent dressing. Moreover, the ability of the alfalfa-based scaffolds to initiate wound healing was compared with that of two types of commercially available wound dressings—hydrocolloid dressing and dermal template dressing. Hydrocolloid is an adhesive gel type dressing for light and moderate wound care, whereas the dermal template is an ECM-based dressing for heavy and hard-to-heal (e.g., chronic ulcers) wound care.[11]

After 14 days of healing, wounds treated with PCL/alfalfa nanofibers or dermal template closed faster than those treated with control, PCL nanofiber, or hydrocolloid dressing (Figure 4b). There was no significant difference in the wound closure rate between PCL/alfalfa nanofibers and dermal templates. To further investigate in vivo tissue regeneration, Masson's trichrome staining was conducted on day 14 tissues (Figure 5a–e). After wounding, epithelial cells migrate to the wound site to close the wounds, whereas fibroblasts and inflammatory cells deposit new ECM components called granulation tissue to fill the wound.[3] Re-epithelialization was measured by calculating the distance among newly formed epithelial layers. In line with the macroscopic wound closure analysis (Figure 4b), the epithelial gaps in PCL/alfalfa nanofiber- or dermal template-treated wounds were significantly smaller than those in control, PCL-only nanofiber-treated, or hydrocolloid-treated wounds (Figure 5f). In addition, more granulation tissue was formed in PCL/alfalfa scaffold-treated wounds than in control and PCL scaffold-treated wounds (Figure 5g). PCL/alfalfa scaffolds and hydrocolloids did not show any significant difference in granulation tissue formation. Compared to all other dressings, the dermal template showed the highest granulation tissue formation.

As previously reported, a statistical STAQ index was utilized to further quantitatively assess the regenerative capability of PCL/alfalfa scaffolds (Figure 5h).[15] The index generates scores from 0 (no overlap with healthy skin) to 100% (perfect overlap with healthy skin). Consequently, this STAQ analysis highlighted the capacity of PCL/alfalfa scaffolds to promote skin restoration, with a 96.9% match to healthy skin in terms of wound closure, re-epithelialization, and granulation tissue formation.

To examine the effects of alfalfa scaffolds on the regeneration of skin appendages such as hair follicles, cytokeratin 14 (K14) staining was performed (Figure 6). K14 is highly expressed in the basal keratinocyte layer and the outer layer of the hair follicle.[72] Here, the formation of new hair follicles in the wound bed was only observed in wounds treated with PCL/alfalfa nanofibers or dermal template with positive K14 staining. Altogether, our in vivo results suggest that PCL/alfalfa nanofiber scaffolds can effectively facilitate tissue repair in mouse skin.

Ex Vivo Human Skin Tissue Regeneration. To further test the regenerative capability of our alfalfa scaffolds, we asked whether PCL/alfalfa nanofiber scaffolds could promote wound healing in human skin. Although animal studies (such as rodent or porcine models) can help to investigate the efficacy of wound dressings, they are unable to fully model the healing processes and outcomes in human skin due to the intrinsic differences between animal and human tissues.[37] Here, wound healing was assessed in a commercially available ex vivo human skin model (NativeSkin, Figure 7a) to compare different fiber samples or dressings.[37] The ex vivo human skin model possesses all types of skin compositions and has little impact on healing processes across different sexes and ages of donors, therefore providing a precise evaluation of healing outcomes prior to clinical trials with humans.[37,73] The tissues were collected from the donor's abdomen, wounded with a 2 mm

DOI: 10.1021/acsami.9b07626
ACS Appl. Mater. Interfaces XXXX, XXX, XXX–XXX

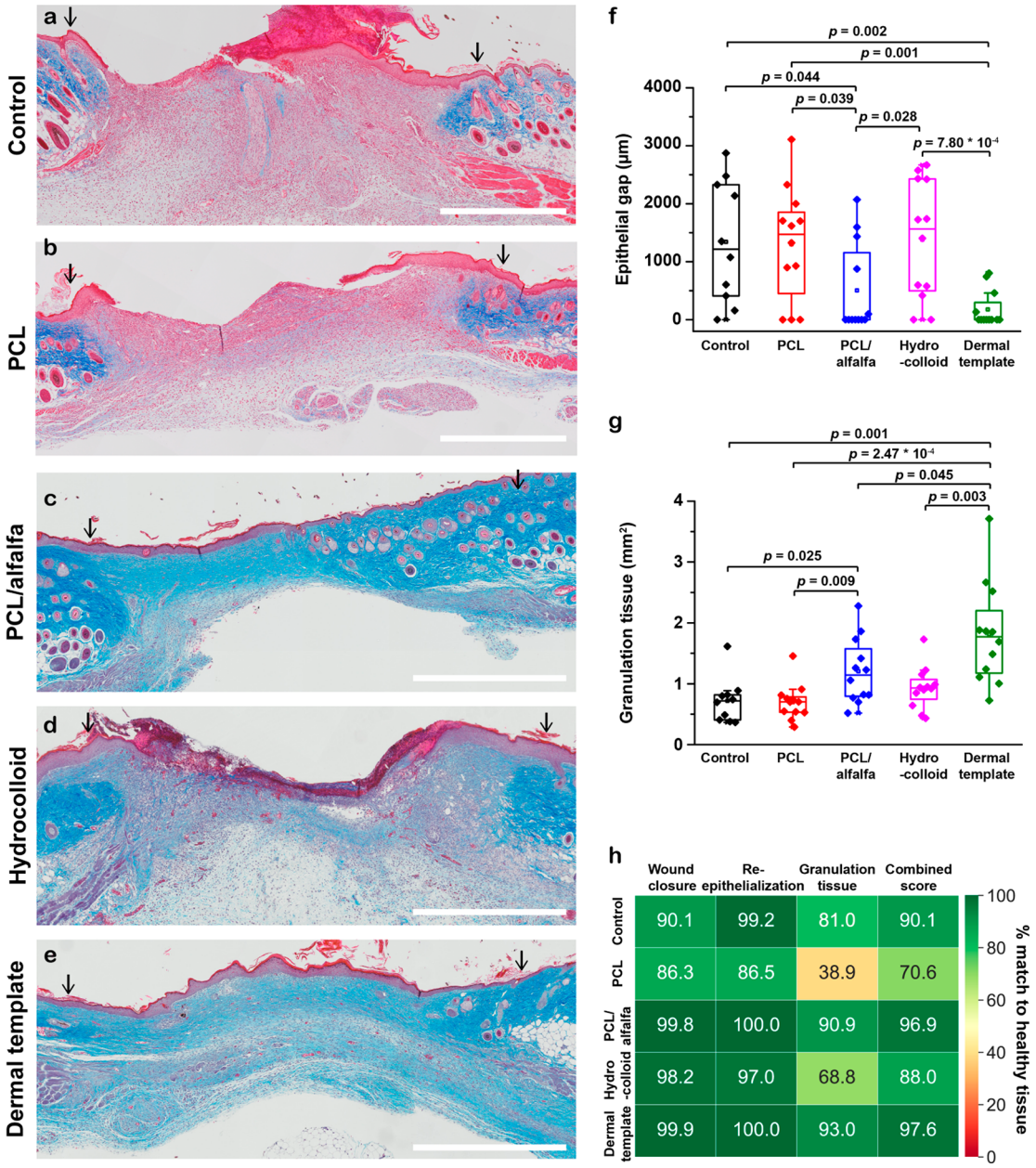

Figure 5. Histological analysis of in vivo mouse skin regeneration. (a–e) Masson's trichrome images of day 14 wounds with (f) epithelial gap and (g) granulation tissue formation analysis. The scale bars are 1 mm. The black arrows indicate the original wound edges. For statistics, $*p < 0.05$, $n = 5$ for control, and $n = 6$ for PCL nanofibers, PCL/alfalfa nanofibers, hydrocolloid, and dermal template (2 sections per tissue). The edges of the box plots in (f) and (g) were defined as the 25th and 75th percentiles. The middle bar is the median, and the whiskers are the 5th and 95th percentiles. (h) Skin tissue architecture quality (STAQ) index to quantitatively compare the efficacy of engineered and commercial dressings, with scores representing the percentage match to healthy skin.

biopsy punch, and embedded in a nourishing gel for up to 7 days of culture, as previously reported.[37] All wound dressings were applied to the wound site, and tissues were harvested after 7 days of culture for histological analysis (Figure 7b). The healing performance in human skin was assessed by the re-epithelialization rate (Figure 7c–h). The epithelial gap in PCL/alfalfa-treated wounds was significantly smaller than that in control or PCL-treated wounds, owing to the existence of an ECM-mimetic fibrous architecture and bioactive alfalfa components. Moreover, the re-epithelialization induced by PCL/alfalfa scaffolds was greater than that induced by hydrocolloids but slower than that induced by the dermal template. However, there were no significant differences in the re-epithelialization rate among PCL/alfalfa scaffolds, hydrocolloids, and dermal templates. These results suggest that PCL/alfalfa scaffolds may be used as a dressing for wound healing in human skin.

DISCUSSION

Because of the complexity of the skin regeneration process and the large number of people suffering from cutaneous damage, wound management continues to be a global healthcare challenge. In the United States alone, 11 million and 6 million people are annually affected by acute and chronic wounds, respectively.[1] In spite of existing treatments and availability of different materials for wound dressings, 28% of wounds are still

DOI: 10.1021/acsami.9b07626
ACS Appl. Mater. Interfaces XXXX, XXX, XXX–XXX

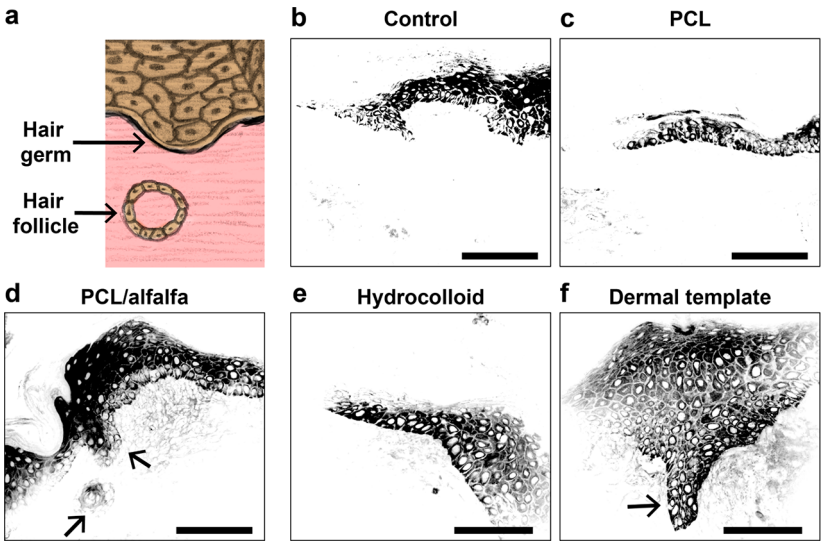

Figure 6. Hair follicle formation in mouse skin. (a) Schematic illustration of hair follicles (cross section) in skin tissues. (b–f) Representative immunofluorescence images (stained against K14) of wound healing and hair follicle formation in mouse models. The arrows in the immunofluorescence images indicate new hair follicle formation at the wound site. The scale bars are 100 μm.

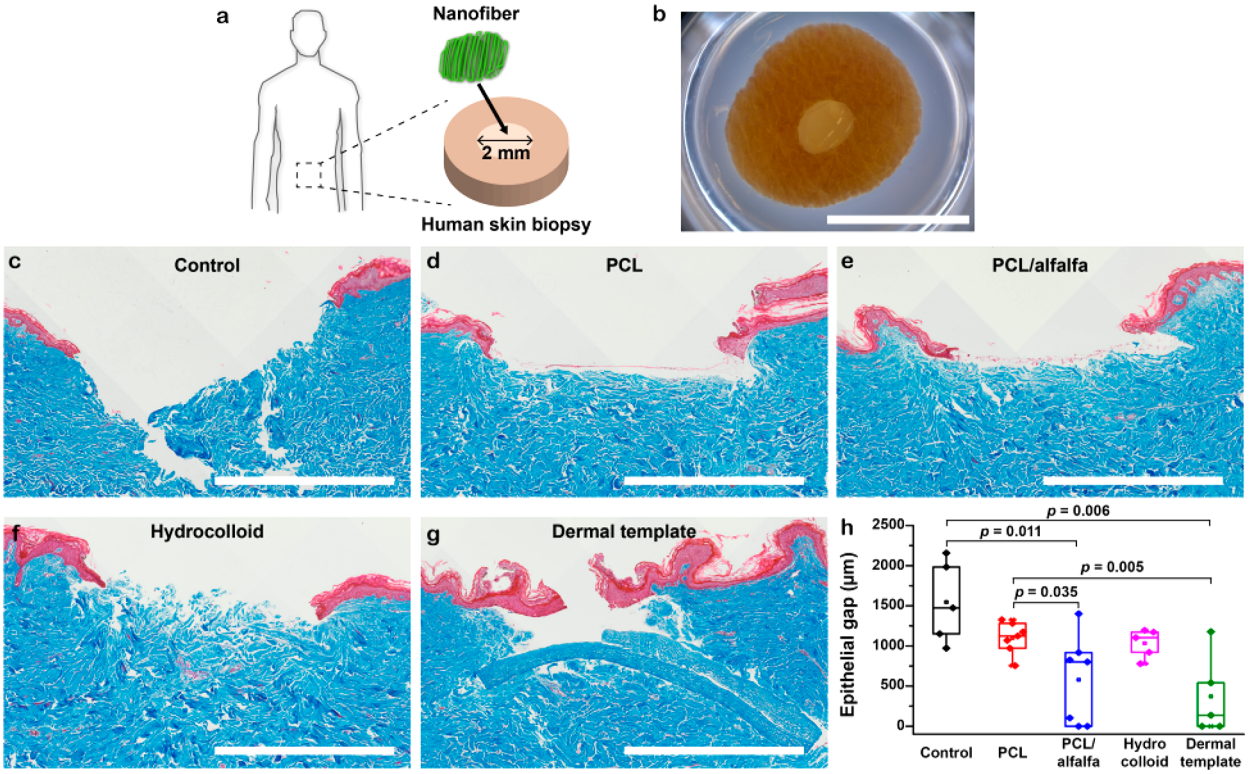

Figure 7. Ex vivo human skin regeneration. (a) Schematic illustration of the ex vivo human skin wound model with (b) a representative image of the wounded human skin model taken from the abdominal area of a donor. The scale bar is 8 mm. (c–g) Masson's trichrome images of day 7 wounds with (h) epithelial gap analysis. The scale bars are 1 mm. For statistics, *$p < 0.05$, $n = 5$ for control, hydrocolloid, and dermal template, $n = 7$ for PCL and PCL/alfalfa nanofibers. The edges of the box plots were defined as the 25th and 75th percentiles. The middle bar is the median, and the whiskers are the 5th and 95th percentiles.

difficult to manage—necessitating development of a new generation of dressings with improved regenerative capabilities.[74] In an effort to address some of the limitations in available wound treatments, we sought to engineer a regenerative nanofiber dressing using a composite material between alfalfa and PCL. Alfalfa is an herbal medicine thought to treat disease, including wound healing.[21,23] It is reported that the chlorophylls and phytoestrogens both contribute to the medicinal effects of alfalfa.[21] We therefore hypothesized that an alfalfa-based bioscaffold may improve wound healing by providing biochemical and topographical cues that can mediate cutaneous regeneration.

Composite nanofibers with alfalfa and PCL were manufactured using a pull spinning system. PCL/alfalfa scaffolds

DOI: 10.1021/acsami.9b07626
ACS Appl. Mater. Interfaces XXXX, XXX, XXX–XXX

successfully recapitulated the native dermal ECM structure and exhibited superhydrophilic surface that could improve cellular growth, moist environment in wound sites, and wound healing.[20,75] After fiber spinning, PCL/alfalfa scaffolds still possessed measurable genistein and chlorophyll content. Because of the existence of alfalfa in the engineered nanofibers, higher HEKa and HNDF adhesion were observed on PCL/alfalfa nanofibers as compared to PCL nanofibers in vitro. Additionally, when tested in a mouse excisional wound splinting model, the performance of PCL/alfalfa scaffolds was then compared with not only internal controls (no treatment and PCL scaffolds) but also commercially available wound dressings (hydrocolloid and dermal template). This comparison was performed in an effort to contribute to the lack of quantitative comparison between new regenerative scaffolds and dressings that serve as clinical standards.[76−78] Hydrocolloid and dermal template were selected as wound dressings for moderate and heavy wound care, respectively.

Hydrocolloid dressings, composed of gel forming colloidal materials with adhesives,[11] are one of the most commonly used dressings to treat light and moderate wounds. These can easily adhere to skin, retain a moist environment, and absorb wound exudate to better promote wound healing as compared with traditional gauze dressings.[11,79] However, hydrocolloid dressings may absorb harmful bacteria due to the adherent nature of the dressings and they lack any bioactive components (e.g., ECM proteins or phytoestrogens). On the other hand, dermal template is a biological or bioactive dressing that actively participates in the healing process to treat heavy acute and chronic wounds.[11] Dermal template is composed of dermal ECM components (mainly collagen), thereby closely mimicking properties of skin tissues.[11] It facilitates wound closure and new cutaneous tissue formation.[80] However, it may induce scar tissue formation composed of excessive collagenous fibers and may cause immunogenicity depending on the donor and recipient species.[20,81] Our engineered wound dressing can recapitulate the nanofibrous architecture of the native skin ECM microenvironment and deliver bioactive molecules (e.g., genistein or chlorophylls) to promote cutaneous tissue repair like dermal template. In addition, similar to hydrocolloid dressings, our plant-based nanofiber scaffolds may pose lower risks of immunogenicity as compared to animal-derived scaffolds.[19,82,83] The PCL/alfalfa nanofibers therefore provide several advantages for better wound care as compared to the aforementioned commercial wound dressings.[47]

To provide a quantitative metric of performance for the new bioscaffold presented herein, skin tissue architecture quality (STAQ) index was applied to compare the healing outcomes based on histological analysis of PCL/alfalfa scaffolds, our controls, and commercially available wound dressings.[15] Considering wound closure, re-epithelialization, and granulation tissue formation, PCL/alfalfa scaffolds scored 96.9% healing, while PCL scaffolds gained 70.6% healing. This data indicated that the existence of bioactive components from alfalfa in the nanofiber scaffolds enhanced healing outcomes. Dermal template and hydrocolloid achieved 97.6% and 88.0% healing, respectively. This suggests that the healing performance of PCL/alfalfa scaffolds falls within the efficacy range of established wound dressings such as hydrocolloid, which mainly provides a barrier against bacterial infection, and dermal template, which delivers bioactive compounds (such as ECM proteins) to enhance skin regeneration.[75]

Finally, the efficacy of our engineered nanofibrous scaffolds was further demonstrated using a commercially available ex vivo human skin model. However, it should be noted that this model can be only cultured up to 7 days, only allowing for re-epithelialization measurements.[37] PCL/alfalfa scaffolds and commercial wound dressings showed improved re-epithelialization as compared to control (no treatment) and PCL scaffolds. However, there was no significant difference between PCL/alfalfa scaffolds, hydrocolloid, and dermal template in healing outcomes in the human skin model. Together with our in vivo data, results measured using the human skin model strongly support that our PCL/alfalfa scaffolds may have wound healing performance similar to commercially available wound dressings.

There are various factors that may contribute to the enhanced wound healing by PCL/alfalfa scaffolds. First, the bioactive components of alfalfa can accelerate the healing process. For instance, genistein (one of the main phytoestrogens) in alfalfa can promote re-epithelialization, new hair follicle formation, and adipose tissue regeneration via ER-β signaling pathways.[25,28,84] Genistein also exhibits antibacterial and anti-inflammatory properties that can prevent bacterial infection, boost inflammatory process, and thus enhance wound healing.[28,85,86] In addition, alfalfa also possesses antibacterial and antimutagenic chlorophylls, which are widely used as additives in commercially available ointments used for treating normal wounds and chronic ulcer.[21,29] Chlorophylls possess a chemical structure similar to that of hemoglobin, which can facilitate oxygenation in wound sites.[30] In addition, the hydrophilic surface, nanofibrous architecture, and mechanical stiffness that mimic the native dermal ECM microenvironment can expedite cell attachment, migration, and consequently ECM remodeling.[52,58−60] Furthermore, the fiber alignment within our engineered scaffolds offers a unidirectional cue to facilitate cell migration and new tissue formation.[48,50]

CONCLUSIONS

In this study, we present an engineered alfalfa-based nanofiber composite material with potential applications toward wound healing. PCL/alfalfa composite bioscaffolds are composed of hydrophilic nanofibers and bioactive compounds such as chlorophylls and genistein, which are known to assist in skin repair. Because of the presence of these medicinal components, aligned PCL/alfalfa nanofiber scaffolds promoted in vitro cellular growth of epidermal keratinocytes and dermal fibroblasts. Furthermore, these alfalfa nanofiber scaffolds showed a regenerative capacity comparable to that of commercially available dressings by promoting wound closure, re-epithelialization, and granulation tissue formation in mice and in human models. In summary, PCL/alfalfa nanofibers can be used to create effective and sustainable regenerative bioscaffolds that may facilitate skin repair by enhancing the rate of wound closure and tissue remodeling.

ASSOCIATED CONTENT

Supporting Information

The Supporting Information is available free of charge on the ACS Publications website at DOI: 10.1021/acsami.9b07626.

SEM image of spun alfalfa (1 wt/v%) solution, PCL/alfalfa (6 wt/v%/1.5 wt/v%), and PCL/alfalfa (6 wt/v %/2 wt/v%); SEM image of healthy mouse skin;

DOI: 10.1021/acsami.9b07626
ACS Appl. Mater. Interfaces XXXX, XXX, XXX−XXX

genistein release profile from PCL/alfalfa scaffolds in PBS solution at 37 °C; LDH cytotoxicity measurements of HEKa cells and HNDFs on nanofibers using the LDH assay at day 7 of cell culture; spinnability of PCL and alfalfa in HFIP by using pull spinning system at different polymer concentrations (PDF)

AUTHOR INFORMATION

Corresponding Author

*Email: kkparker@seas.harvard.edu. Tel.:+1- 617-495-1102.

ORCID

Herdeline Ann M. Ardoña: 0000-0003-0640-1262

Kevin Kit Parker: 0000-0002-5968-7535

Author Contributions

The manuscript was written through the contributions of all authors. All authors have given approval to the final version of the manuscript.

Notes

The authors declare no competing financial interest.

ACKNOWLEDGMENTS

This work was supported by the Wyss Institute for Biologically Inspired Engineering at Harvard University. This research was also performed in part at the Center for Nanoscale Systems (CNS), a member of the National Nanotechnology Infrastructure Network (NNIN), which is supported by the National Science Foundation under NSF Award 1541959. CNS is part of Harvard University. This study was partly supported by the Harvard University Materials Research Science and Engineering Center (MRSEC), NSF Award DMR-1420570. We thank the Dana-Farber/Harvard Cancer Center in Boston, MA, for the use of the Specialized Histopathology Core, which provided tissue preparation and histological staining services. The Dana-Farber/Harvard Cancer Center is supported in part by an NCI Cancer Center Support Grant (NIH 5 P30 CA06516). We thank the Neurobiology Department and the Neurobiology Imaging Facility for consultation and instrument availability that supported this work. This facility is supported in part by the Neural Imaging Center as part of an NINDS P30 Core Center grant (NS072030). H.A.M.A. would like to thank the American Chemical Society for generous support through the Irving S. Sigal Postdoctoral Fellowship. The authors thank Dr. Sean P. Sheehy for providing the Python code to run the quality index and Dr. John F. Zimmerman for helpful comments. The authors also appreciate the graphics provided by Su-Yeon Choi and Michael Rosnach.

REFERENCES

(1) Demidova-Rice, T. N.; Hamblin, M. R.; Herman, I. M. Acute and Impaired Wound Healing: Pathophysiology and Current Methods for Drug Delivery, Part 1: Normal and Chronic Wounds: Biology, Causes, and Approaches to Care. *Adv. Skin Wound Care* **2012**, *25* (7), 304.

(2) Han, G.; Ceilley, R. Chronic Wound Healing: A Review of Current Management and Treatments. *Adv. Ther.* **2017**, *34* (3), 599–610.

(3) Martin, P. Wound Healing–Aiming for Perfect Skin Regeneration. *Science* **1997**, *276* (5309), 75–81.

(4) Chantre, C. O.; Hoerstrup, S. P.; Parker, K. K. Engineering Biomimetic and Instructive Materials for Wound Healing and Regeneration. *Curr. Opin Biomed Eng.* **2019**, *10*, 97–106.

(5) Plikus, M. V.; Guerrero-Juarez, C. F.; Ito, M.; Li, Y. R.; Dedhia, P. H.; Zheng, Y.; Shao, M.; Gay, D. L.; Ramos, R.; Hsi, T.-C.; et al. Regeneration of Fat Cells from Myofibroblasts During Wound Healing. *Science* **2017**, *355* (6326), 748–752.

(6) Dvir, T.; Timko, B. P.; Kohane, D. S.; Langer, R. Nanotechnological Strategies for Engineering Complex Tissues. *Nat. Nanotechnol.* **2011**, *6* (1), 13.

(7) Wang, S. Y.; Kim, H.; Kwak, G.; Yoon, H. Y.; Jo, S. D.; Lee, J. E.; Cho, D.; Kwon, I. C.; Kim, S. H. Development of Biocompatible Ha Hydrogels Embedded with a New Synthetic Peptide Promoting Cellular Migration for Advanced Wound Care Management. *Adv. Sci.* **2018**, *5* (11), 1800852.

(8) Lai, B. Q.; Feng, B.; Che, M. T.; Wang, L. J.; Cai, S.; Huang, M. Y.; Gu, H. Y.; Jiang, B.; Ling, E. A.; Li, M.; et al. A Modular Assembly of Spinal Cord–Like Tissue Allows Targeted Tissue Repair in the Transected Spinal Cord. *Adv. Sci.* **2018**, *5* (9), 1800261.

(9) Mao, X.; Cheng, R.; Zhang, H.; Bae, J.; Cheng, L.; Zhang, L.; Deng, L.; Cui, W.; Zhang, Y.; Santos, H. A.; Sun, X. Self-Healing and Injectable Hydrogel for Matching Skin Flap Regeneration. *Adv. Sci.* **2019**, *6* (3), 1801555.

(10) Darling, N. J.; Sideris, E.; Hamada, N.; Carmichael, S. T.; Segura, T. Injectable and Spatially Patterned Microporous Annealed Particle (Map) Hydrogels for Tissue Repair Applications. *Adv. Sci.* **2018**, *5* (11), 1801046.

(11) Boateng, J. S.; Matthews, K. H.; Stevens, H. N.; Eccleston, G. M. Wound Healing Dressings and Drug Delivery Systems: A Review. *J. Pharm. Sci.* **2008**, *97* (8), 2892–2923.

(12) Li, W. J.; Laurencin, C. T.; Caterson, E. J.; Tuan, R. S.; Ko, F. K. Electrospun Nanofibrous Structure: A Novel Scaffold for Tissue Engineering. *J. Biomed. Mater. Res.* **2002**, *60* (4), 613–621.

(13) Ji, Y.; Xiao, Y.; Xu, L.; He, J.; Qian, C.; Li, W.; Wu, L.; Chen, R.; Wang, J.; Hu, R.; et al. Drug-Bearing Supramolecular Mmp Inhibitor Nanofibers for Inhibition of Metastasis and Growth of Liver Cancer. *Adv. Sci.* **2018**, *5* (8), 1700867.

(14) Ding, Y.; Li, W.; Zhang, F.; Liu, Z.; Zanjanizadeh Ezazi, N.; Liu, D.; Santos, H. A. Electrospun Fibrous Architectures for Drug Delivery, Tissue Engineering and Cancer Therapy. *Adv. Funct. Mater.* **2019**, *29* (2), 1802852.

(15) Chantre, C. O.; Campbell, P. H.; Golecki, H. M.; Buganza, A. T.; Capulli, A. K.; Deravi, L. F.; Dauth, S.; Sheehy, S. P.; Paten, J. A.; Gledhill, K.; Doucet, Y. S.; Abaci, H. E.; Ahn, S.; Pope, B. D.; Ruberti, J. W.; Hoerstrup, S. P.; Christiano, A. M.; Parker, K. K. Production-Scale Fibronectin Nanofibers Promote Wound Closure and Tissue Repair in a Dermal Mouse Model. *Biomaterials* **2018**, *166*, 96–108.

(16) Ma, P. X. Biomimetic Materials for Tissue Engineering. *Adv. Drug Delivery Rev.* **2008**, *60* (2), 184–198.

(17) Chan, G.; Mooney, D. J. New Materials for Tissue Engineering: Towards Greater Control over the Biological Response. *Trends Biotechnol.* **2008**, *26* (7), 382–392.

(18) Gjorevski, N.; Sachs, N.; Manfrin, A.; Giger, S.; Bragina, M. E.; Ordóñez-Morán, P.; Clevers, H.; Lutolf, M. P. Designer Matrices for Intestinal Stem Cell and Organoid Culture. *Nature* **2016**, *539* (7630), 560.

(19) Reddy, N.; Yang, Y. Potential of Plant Proteins for Medical Applications. *Trends Biotechnol.* **2011**, *29* (10), 490–498.

(20) Ahn, S.; Chantre, C. O.; Gannon, A. R.; Lind, J. U.; Campbell, P. H.; Grevesse, T.; O'Connor, B. B.; Parker, K. K. Soy Protein/Cellulose Nanofiber Scaffolds Mimicking Skin Extracellular Matrix for Enhanced Wound Healing. *Adv. Healthcare Mater.* **2018**, *7* (9), 1701175.

(21) Bora, K. S.; Sharma, A. Phytochemical and Pharmacological Potential of Medicago Sativa: A Review. *Pharm. Biol.* **2011**, *49* (2), 211–220.

(22) Xie, Y.; Wang, L.; Sun, H.; Wang, Y.; Yang, Z.; Zhang, G.; Jiang, S.; Yang, W. Polysaccharide from Alfalfa Activates Raw 264.7 Macrophages through Mapk and Nf-Kb Signaling Pathways. *Int. J. Biol. Macromol.* **2019**, *126*, 960–968.

DOI: 10.1021/acsami.9b07626
ACS Appl. Mater. Interfaces XXXX, XXX, XXX–XXX

(23) Kargozar, R.; Azizi, H.; Salari, R. A Review of Effective Herbal Medicines in Controlling Menopausal Symptoms. *Electron Physician* **2017**, *9* (11), 5826.
(24) Patisaul, H. B.; Jefferson, W. The Pros and Cons of Phytoestrogens. *Front. Neuroendocrinol.* **2010**, *31* (4), 400−419.
(25) Zhao, J.; Harada, N.; Kurihara, H.; Nakagata, N.; Okajima, K. Dietary Isoflavone Increases Insulin-Like Growth Factor-I Production, Thereby Promoting Hair Growth in Mice. *J. Nutr. Biochem.* **2011**, *22* (3), 227−233.
(26) Campbell, L.; Emmerson, E.; Davies, F.; Gilliver, S. C.; Krust, A.; Chambon, P.; Ashcroft, G. S.; Hardman, M. J. Estrogen Promotes Cutaneous Wound Healing Via Estrogen Receptor B Independent of Its Antiinflammatory Activities. *J. Exp. Med.* **2010**, *207* (9), 1825−1833.
(27) Ashcroft, G. S.; Dodsworth, J.; Van Boxtel, E.; Tarnuzzer, R. W.; Horan, M. A.; Schultz, G. S.; Ferguson, M. W.J. Estrogen Accelerates Cutaneous Wound Healing Associated with an Increase in Tgf-B1 Levels. *Nat. Med.* **1997**, *3* (11), 1209−1215.
(28) Emmerson, E.; Campbell, L.; Ashcroft, G. S.; Hardman, M. J. The Phytoestrogen Genistein Promotes Wound Healing by Multiple Independent Mechanisms. *Mol. Cell. Endocrinol.* **2010**, *321* (2), 184−193.
(29) Carpenter, E. B. Clinical Experiences with Chlorophyll Preparations: With Particular Reference to Chronic Osteomyelitis and Chronic Ulcers. *Am. J. Surg.* **1949**, *77* (2), 167−171.
(30) Hosikian, A.; Lim, S.; Halim, R.; Danquah, M. K. Chlorophyll Extraction from Microalgae: A Review on the Process Engineering Aspects. *Int. J. Chem. Eng.* **2010**, *2010*, 1−11.
(31) Deravi, L. F.; Sinatra, N. R.; Chantre, C. O.; Nesmith, A. P.; Yuan, H.; Deravi, S. K.; Goss, J. A.; MacQueen, L. A.; Badrossamy, M. R.; Gonzalez, G. M.; Phillips, M. D.; Parker, K. K. Design and Fabrication of Fibrous Nanomaterials Using Pull Spinning. *Macromol. Mater. Eng.* **2017**, *302* (3), 1600404.
(32) Hotaling, N. A.; Bharti, K.; Kriel, H.; Simon, C. G. Diameterj: A Validated Open Source Nanofiber Diameter Measurement Tool. *Biomaterials* **2015**, *61*, 327−338.
(33) Rezakhaniha, R.; Agianniotis, A.; Schrauwen, J. T. C.; Griffa, A.; Sage, D.; Bouten, C. v.; Van de Vosse, F.; Unser, M.; Stergiopulos, N. Experimental Investigation of Collagen Waviness and Orientation in the Arterial Adventitia Using Confocal Laser Scanning Microscopy. *Biomech. Model. Mechanobiol.* **2012**, *11* (3−4), 461−473.
(34) Stalder, A.; Kulik, G.; Sage, D.; Barbieri, L.; Hoffmann, P. A Snake-Based Approach to Accurate Determination of Both Contact Points and Contact Angles. *Colloids Surf., A* **2006**, *286* (1−3), 92−103.
(35) Korzeniewski, C.; Callewaert, D. M. An Enzyme-Release Assay for Natural Cytotoxicity. *J. Immunol. Methods* **1983**, *64* (3), 313−320.
(36) Wang, X.; Ge, J.; Tredget, E. E.; Wu, Y. The Mouse Excisional Wound Splinting Model, Including Applications for Stem Cell Transplantation. *Nat. Protoc.* **2013**, *8* (2), 302.
(37) De Wever, B.; Kurdykowski, S.; Descargues, P. Human Skin Models for Research Applications in Pharmacology and Toxicology: Introducing Nativeskin®, the "Missing Link" Bridging Cell Culture and/or Reconstructed Skin Models and Human Clinical Testing. *Applied In Vitro Toxicology* **2015**, *1* (1), 26−32.
(38) Badrossamay, M. R.; McIlwee, H. A.; Goss, J. A.; Parker, K. K. Nanofiber Assembly by Rotary Jet-Spinning. *Nano Lett.* **2010**, *10* (6), 2257−2261.
(39) Mellado, P.; McIlwee, H. A.; Badrossamay, M. R.; Goss, J. A.; Mahadevan, L.; Parker, K. K. A Simple Model for Nanofiber Formation by Rotary Jet-Spinning. *Appl. Phys. Lett.* **2011**, *99* (20), 203107.
(40) Golecki, H. M.; Yuan, H.; Glavin, C.; Potter, B.; Badrossamay, M. R.; Goss, J. A.; Phillips, M. D.; Parker, K. K. Effect of Solvent Evaporation on Fiber Morphology in Rotary Jet Spinning. *Langmuir* **2014**, *30* (44), 13369−13374.
(41) Capulli, A.; MacQueen, L.; Sheehy, S. P.; Parker, K. Fibrous Scaffolds for Building Hearts and Heart Parts. *Adv. Drug Delivery Rev.* **2016**, *96*, 83−102.
(42) Ahn, S.; Ardona, H. A. M.; Lind, J. U.; Eweje, F.; Kim, S. L.; Gonzalez, G. M.; Liu, Q.; Zimmerman, J. F.; Pyrgiotakis, G.; Zhang, Z.; Beltran-Huarac, J.; Carpinone, P.; Moudgil, B. M.; Demokritou, P.; Parker, K. K. Mussel-Inspired 3d Fiber Scaffolds for Heart-on-a-Chip Toxicity Studies of Engineered Nanomaterials. *Anal. Bioanal. Chem.* **2018**, *410* (24), 6141−6154.
(43) Gonzalez, G. M.; MacQueen, L. A.; Lind, J. U.; Fitzgibbons, S. A.; Chantre, C. O.; Huggler, I.; Golecki, H. M.; Goss, J. A.; Parker, K. K. Production of Synthetic, Para-Aramid and Biopolymer Nanofibers by Immersion Rotary Jet-Spinning. *Macromol. Mater. Eng.* **2017**, *302* (1), 1600365.
(44) Capulli, A. K.; Emmert, M. Y.; Pasqualini, F. S.; Kehl, D.; Caliskan, E.; Lind, J. U.; Sheehy, S. P.; Park, S. J.; Ahn, S.; Weber, B.; Goss, J. A.; Hoerstrup, S. P.; Parker, K. K. Jetvalve: Rapid Manufacturing of Biohybrid Scaffolds for Biomimetic Heart Valve Replacement. *Biomaterials* **2017**, *133*, 229−241.
(45) MacQueen, L. A.; Sheehy, S. P.; Chantre, C. O.; Zimmerman, J. F.; Pasqualini, F. S.; Liu, X.; Goss, J. A.; Campbell, P. H.; Gonzalez, G. M.; Park, S. J.; Capulli, A. K.; Ferrier, J. P.; Kosar, T. F.; Mahadevan, L.; Pu, W. T.; Parker, K. K. A Tissue-Engineered Scale Model of the Heart Ventricle. *Nat. Biomed Eng.* **2018**, *2* (12), 930−941.
(46) Suwantong, O. Biomedical Applications of Electrospun Polycaprolactone Fiber Mats. *Polym. Adv. Technol.* **2016**, *27* (10), 1264−1273.
(47) Zahedi, P.; Rezaeian, I.; Ranaei-Siadat, S. O.; Jafari, S. H.; Supaphol, P. A Review on Wound Dressings with an Emphasis on Electrospun Nanofibrous Polymeric Bandages. *Polym. Adv. Technol.* **2009**, *21* (2), 77−95.
(48) Sell, S.; Barnes, C.; Smith, M.; McClure, M.; Madurantakam, P.; Grant, J.; Mcmanus, M.; Bowlin, G. Extracellular Matrix Regenerated: Tissue Engineering Via Electrospun Biomimetic Nanofibers. *Polym. Int.* **2007**, *56* (11), 1349−1360.
(49) Yang, W.; Sherman, V. R.; Gludovatz, B.; Schaible, E.; Stewart, P.; Ritchie, R. O.; Meyers, M. A. On the Tear Resistance of Skin. *Nat. Commun.* **2015**, *6*, 6649.
(50) Badrossamay, M. R.; Balachandran, K.; Capulli, A. K.; Golecki, H. M.; Agarwal, A.; Goss, J. A.; Kim, H.; Shin, K.; Parker, K. K. Engineering Hybrid Polymer-Protein Super-Aligned Nanofibers Via Rotary Jet Spinning. *Biomaterials* **2014**, *35* (10), 3188−3197.
(51) Discher, D. E.; Janmey, P.; Wang, Y.-l. Tissue Cells Feel and Respond to the Stiffness of Their Substrate. *Science* **2005**, *310* (5751), 1139−1143.
(52) Wells, R. G. The Role of Matrix Stiffness in Regulating Cell Behavior. *Hepatology* **2008**, *47* (4), 1394−1400.
(53) Barnes, J. M.; Przybyla, L.; Weaver, V. M. Tissue Mechanics Regulate Brain Development, Homeostasis and Disease. *J. Cell Sci.* **2017**, *130* (1), 71−82.
(54) Pan, J.-f.; Liu, N.-h.; Sun, H.; Xu, F. Preparation and Characterization of Electrospun Plcl/Poloxamer Nanofibers and Dextran/Gelatin Hydrogels for Skin Tissue Engineering. *PLoS One* **2014**, *9* (11), e112885.
(55) Liang, X.; Boppart, S. A. Biomechanical Properties of in Vivo Human Skin from Dynamic Optical Coherence Elastography. *IEEE Trans. Biomed. Eng.* **2010**, *57* (4), 953−959.
(56) Pailler-Mattei, C.; Bec, S.; Zahouani, H. In Vivo Measurements of the Elastic Mechanical Properties of Human Skin by Indentation Tests. *Med. Eng. Phys.* **2008**, *30* (5), 599−606.
(57) Hashizume, R.; Fujimoto, K. L.; Hong, Y.; Amoroso, N. J.; Tobita, K.; Miki, T.; Keller, B. B.; Sacks, M. S.; Wagner, W. R. Morphological and Mechanical Characteristics of the Reconstructed Rat Abdominal Wall Following Use of a Wet Electrospun Biodegradable Polyurethane Elastomer Scaffold. *Biomaterials* **2010**, *31* (12), 3253−3265.
(58) Dabiri, G.; Damstetter, E.; Phillips, T. Choosing a Wound Dressing Based on Common Wound Characteristics. *Adv. Wound Care* **2016**, *5* (1), 32−41.
(59) Liu, X.; Lin, T.; Fang, J.; Yao, G.; Zhao, H.; Dodson, M.; Wang, X. In Vivo Wound Healing and Antibacterial Performances of

DOI: 10.1021/acsami.9b07626
ACS Appl. Mater. Interfaces XXXX, XXX, XXX−XXX

Electrospun Nanofibre Membranes. *J. Biomed. Mater. Res., Part A* **2010**, *94* (2), 499−508.
(60) Webb, K.; Hlady, V.; Tresco, P. A. Relative Importance of Surface Wettability and Charged Functional Groups on Nih 3t3 Fibroblast Attachment, Spreading, and Cytoskeletal Organization. *J. Biomed. Mater. Res.* **1998**, *41* (3), 422−430.
(61) Yoo, H. S.; Kim, T. G.; Park, T. G. Surface-Functionalized Electrospun Nanofibers for Tissue Engineering and Drug Delivery. *Adv. Drug Delivery Rev.* **2009**, *61* (12), 1033−1042.
(62) Xu, X.; Jiang, L.; Zhou, Z.; Wu, X.; Wang, Y. Preparation and Properties of Electrospun Soy Protein Isolate/Polyethylene Oxide Nanofiber Membranes. *ACS Appl. Mater. Interfaces* **2012**, *4* (8), 4331−4337.
(63) Hu, J.; Prabhakaran, M. P.; Tian, L.; Ding, X.; Ramakrishna, S. Drug-Loaded Emulsion Electrospun Nanofibers: Characterization, Drug Release and in Vitro Biocompatibility. *RSC Adv.* **2015**, *5* (121), 100256−100267.
(64) Buddhiranon, S.; DeFine, L. A.; Alexander, T. S.; Kyu, T. Genistein-Modified Poly (Ethylene Oxide)/Poly (D, L-Lactic Acid) Electrospun Mats with Improved Antioxidant and Anti-Inflammatory Properties. *Biomacromolecules* **2013**, *14* (5), 1423−1433.
(65) Ibrahim, S.; Sayed, H. M.; El-Rafei, A.; El Amir, A.; Ismail, M.; Allam, N. K. Improved Genistein Loading and Release on Electrospun Chitosan Nanofiber Blends. *J. Mol. Liq.* **2016**, *223*, 1056−1061.
(66) Yi, Y.; Kermasha, S.; L'Hocine, L.; Neufeld, R. Encapsulation of Chlorophyllase in Hydrophobically Modified Hydrogel. *J. Mol. Catal. B: Enzym.* **2002**, *19*, 319−325.
(67) Mandal, P.; Manna, J. S.; Das, D.; Mitra, M. K. Excitonic Dynamics of Chlorophyll-a Molecules in Chitosan Hydrogel Scaffold. *Photochem. Photobiol. Sci.* **2015**, *14* (4), 786−791.
(68) Li, H.; Liu, J.; Li, D.; Wang, H. Study on Separation and Purification of Genistein in the Soybean Residue Using Macroporous Resin Adsorption. *Ind. Eng. Chem. Res.* **2012**, *51* (1), 44−49.
(69) Lichtenthaler, H. K.; Buschmann, C. Chlorophylls and Carotenoids: Measurement and Characterization by Uv-Vis Spectroscopy. *Current Protocols in Food Analytical Chemistry* **2001**, *1* (1), F4.3.1−F4.3.8.
(70) Zhang, Q.; Oh, J.-H.; Park, C. H.; Baek, J.-H.; Ryoo, H.-M.; Woo, K. M. Effects of Dimethyloxalylglycine-Embedded Poly (E-Caprolactone) Fiber Meshes on Wound Healing in Diabetic Rats. *ACS Appl. Mater. Interfaces* **2017**, *9* (9), 7950−7963.
(71) Muhamed, I.; Sproul, E. P.; Ligler, F. S.; Brown, A. C. Fibrin Nanoparticles Coupled with Keratinocyte Growth Factor Enhance the Dermal Wound-Healing Rate. *ACS Appl. Mater. Interfaces* **2019**, *11* (4), 3771−3780.
(72) Nijhof, J. G.; Braun, K. M.; Giangreco, A.; van Pelt, C.; Kawamoto, H.; Boyd, R. L.; Willemze, R.; Mullenders, L. H.; Watt, F. M.; de Gruijl, F. R. The Cell-Surface Marker Mts24 Identifies a Novel Population of Follicular Keratinocytes with Characteristics of Progenitor Cells. *Development* **2006**, *133* (15), 3027−3037.
(73) Boekema, B.; Ulrich, M. M.; Middelkoop, E. Models for Cutaneous Wound Healing. *Wound Repair Regen.* **2017**, *25* (2), 347−348.
(74) McCaughan, D.; Sheard, L.; Cullum, N.; Dumville, J.; Chetter, I. Patients' Perceptions and Experiences of Living with a Surgical Wound Healing by Secondary Intention: A Qualitative Study. *Int. J. Nurs. Stud.* **2018**, *77*, 29−38.
(75) Dhivya, S.; Padma, V. V.; Santhini, E. Wound Dressings−a Review. *Biomedicine* **2015**, *5* (4), 24−28.
(76) Hassiba, A. J.; El Zowalaty, M. E.; Nasrallah, G. K.; Webster, T. J.; Luyt, A. S.; Abdullah, A. M.; Elzatahry, A. A. Review of Recent Research on Biomedical Applications of Electrospun Polymer Nanofibers for Improved Wound Healing. *Nanomedicine* **2016**, *11* (6), 715−737.
(77) Zhu, J.; Li, F.; Wang, X.; Yu, J.; Wu, D. Hyaluronic Acid and Polyethylene Glycol Hybrid Hydrogel Encapsulating Nanogel with Hemostasis and Sustainable Antibacterial Property for Wound Healing. *ACS Appl. Mater. Interfaces* **2018**, *10* (16), 13304−13316.
(78) Lu, G.; Ding, Z.; Wei, Y.; Lu, X.; Lu, Q.; Kaplan, D. L. Anisotropic Biomimetic Silk Scaffolds for Improved Cell Migration and Healing of Skin Wounds. *ACS Appl. Mater. Interfaces* **2018**, *10* (51), 44314−44323.
(79) Hoekstra, M.; Hermans, M.; Richters, C.; Dutrieux, R. A Histological Comparison of Acute Inflammatory Responses with a Hydrofibre or Tulle Gauze Dressing. *J. Wound Care* **2002**, *11* (3), 113−117.
(80) Sai K, P.; Babu, M. Collagen Based Dressings–a Review. *Burns* **2000**, *26* (1), 54−62.
(81) Lynn, A.; Yannas, I.; Bonfield, W. Antigenicity and Immunogenicity of Collagen. *J. Biomed. Mater. Res.* **2004**, *71B* (2), 343−354.
(82) Li, Z.; Tan, B. H. Towards the Development of Polycaprolactone Based Amphiphilic Block Copolymers: Molecular Design, Self-Assembly and Biomedical Applications. *Mater. Sci. Eng., C* **2014**, *45*, 620−634.
(83) Willard, J. J.; Drexler, J. W.; Das, A.; Roy, S.; Shilo, S.; Shoseyov, O.; Powell, H. M. Plant-Derived Human Collagen Scaffolds for Skin Tissue Engineering. *Tissue Eng., Part A* **2013**, *19* (13−14), 1507−1518.
(84) Zanella, I.; Marrazzo, E.; Biasiotto, G.; Penza, M.; Romani, A.; Vignolini, P.; Caimi, L.; Di Lorenzo, D. Soy and the Soy Isoflavone Genistein Promote Adipose Tissue Development in Male Mice on a Low-Fat Diet. *Eur. J. Nutr.* **2015**, *54* (7), 1095−1107.
(85) Hong, H.; Landauer, M. R.; Foriska, M. A.; Ledney, G. D. Antibacterial Activity of the Soy Isoflavone Genistein. *J. Basic Microbiol.* **2006**, *46* (4), 329−335.
(86) Verdrengh, M.; Jonsson, I.; Holmdahl, R.; Tarkowski, A. Genistein as an Anti-Inflammatory Agent. *Inflammation Res.* **2003**, *52* (8), 341−346.

DOI: 10.1021/acsami.9b07626
ACS Appl. Mater. Interfaces XXXX, XXX, XXX−XXX